Journal of
Nanoscience and Nanotechnology
Vol. 11, 1–6, 2011

Vanadium Oxide Nanoparticles as Optical Sensors of Cysteine

W. Celestino-Santos[1], A. G. Bezerra, Jr.[2], A. B. Cezar[1], N. Mattoso[1], and W. H. Schreiner[1,*]

[1] *Departamento de Física, Universidade Federal do Paraná, Centro Politécnico, Jardim das Américas, 81531-880, Curitiba, Paraná, Brazil*
[2] *Departamento Acadêmico de Física, Universidade Tecnológica Federal do Paraná, Avenida Sete de Setembro, 3165, Centro, 80230-010, Curitiba, Paraná, Brazil*

We report on the synthesis of vanadium oxide nanoparticles using the laser ablation in solution technique. The particles were characterized by dynamic light scattering-DLS, transmission electron microscopy-TEM, X-ray diffraction-XRD, X-ray photoelectron spectroscopy-XPS and UV-Vis optical spectroscopy. The oxide nanoparticles are mainly composed of tetragonal V_2O_5, a semiconductor with a 2.2 eV band gap. The interaction of the nanoparticles with cysteine, a very important aminoacid present in proteins, was studied. Upon reaction with cysteine, the bandgap of the nanoparticles shifts to the ultraviolet region at 2.87 eV. This color change from yellow to transparent can be used for selective cysteine sensing. Additionally, the intervalence band of the optical absorption spectra shows capability for cysteine sensing in the μM range.

Keywords:

RESEARCH ARTICLE

1. INTRODUCTION

Vanadium oxides have many properties which have been used in several different areas of applications. For the Physicist, vanadium oxides present a wealth of interesting features. The phase diagram of the vanadium-oxygen system shows some twenty oxides with many different structures.[1] Several of these oxides present metal-insulator or semiconductor-insulator transitions, with peculiar electronic, magnetic and structural behavior, which are only partially understood. Thermochromic behavior has been reported for VO_2[2] and vanadium oxides are also considered as materials for solar energy harvesting[3] as well as for electrochromic applications.[4] For the Chemist, vanadium oxides are important for their catalytical applications in many industries. These catalytic properties are based on two aspects: vanadium oxides have a variety of oxidation states, ranging from 2^+ to 5^+, and a great variability of oxygen coordination geometries. For the Biologist, vanadium and vanadium oxides have important action in proteins and biological materials. This has applications in medicine for the treatment of cancer tumors.

Vanadium oxide nanoparticles have been produced in several ways. Laser pyrolysis,[5] pulsed laser deposition (PLD),[6] sol–gel,[7,8] chemical vapor deposition (CVD) and sputtering,[9] co-implantation[10] and microwave plasma decomposition[11] have been used as synthesis routes.

Laser ablation synthesis in solution, LASiS, emerged in the last years as an alternative to the traditional techniques for nanoparticle production.[12] Nanoparticles are formed during the abrupt collapse of the plasma generated by a laser pulse with a target located in a liquid. The control of nanoparticle size is one of the major problems associated to LASiS. The nanoparticles can be obtained in water or solvents without stabilizing molecules. Probably, LASiS is one of the easiest routes for nanoparticle production.

Here we report on the LASiS production of vanadium oxide nanoparticles in water, their characterization and their interaction with cysteine. Cysteine is one of the 20 aminoacids found in proteins. Cysteine has a thiol sidechain and is the main representative of thiols in Biology. The functionalization of noble metals with cysteine has been repeatedly studied (see e.g. Ref. [13] and references therein).

2. EXPERIMENTAL DETAILS

A Q-switched Quantronix Model 117 Nd:YAG laser, operating at 300 Hz and delivering 150 ns pulses at 1064 nm was used in the experiments. The laser beam was focused with a 50 mm lens on a vanadium target, Williams Advanced Materials 2N7, producing a 40 μm spotsize.

*Author to whom correspondence should be addressed.

The laser fluence was of 8.11×10^5 J/m^2. The target was placed 2 mm under bi-distilled water with a pH of 8.25 and the total water amount was maintained at 2 ml. The irradiation time was of 10 minutes. We estimate the total amount of removed vanadium from the target by this process at 1.08 mg, which would amount to a suspension of 10.6 mM vanadium in water. The suspension had a final pH of 4.

The nanoparticle size distribution was measured using a dynamic light scattering equipment, Brookhaven BI-200SM, ver. 2.0, which employs a 632.8 nm, 75 mW, CW HeNe laser.

Transmission electron microscopy-TEM was done on a JEOL JEM-1200 E.M. II microscope operating at 120 kV. The nanoparticle suspension was deposited on a commercial copper grid and left to dry. Electron diffraction on selected nanoparticles was done and a diffraction pattern of a polycrystalline gold thin film was used for calibration.

X-ray diffraction-XRD was done using Shimadzu XRD-7000 equipment operating with 40 kV and 30 mA emission in Bragg-Brentano geometry with Cu K_α radiation.

X-ray photoelectron spectroscopy-XPS was done using a VGMicrotech ESCA3000 spectrometer with a base pressure of 3×10^{-10} mbar, a 250 mm semi-hemispherical analyzer and 9 channeltron detectors. The X-ray source operated at 15 kV and 20 mA emission. Non monochromatic Al K_α X-rays were used. The overall resolution of the spectrometer was of 0.8 eV. The samples were prepared depositing the nanoparticle suspension on naturally oxidized Si(111) wafers and left to dry. The Si_{2p} signals as well as the O_{1s} signal from SiO_2 in the spectra were used for energy calibration. The analysis of the spectra was done, subtracting the background using Shirley, and the deconvolution was done using software developed by XPS International.[15]

The UV-Vis spectra were obtained on a Spectro Vision Model DB-1880 S spectrometer in the absorption mode, from 280 nm to 1100 nm. 10 mm thick quartz couvettes were used for the nanoparticle suspension.

Cysteine, $C_3H_7NO_2S$, Sygma-Aldrich Corporation 99%, was added to the yellowish nanoparticle suspension. Different additions of cysteine were tested, especially for the UV-Vis measurements.

2.1. Nanoparticle Characterization

Figure 1 shows the size distribution for the vanadium oxide nanoparticles. The particles have two fairly large distributions around 10 and 60 nm.

Figure 2(a) shows a TEM image of a vanadium oxide nanoparticle of ∼150 nm. Clearly an outer shell surrounds the inner core of the particle. The inner crystallites are of 8–20 nm and the external amorphous layer has a width of approximately 30 nm.

The electron diffraction pattern of the same nanoparticle is shown on Figure 2(b). The spots can be indexed to the

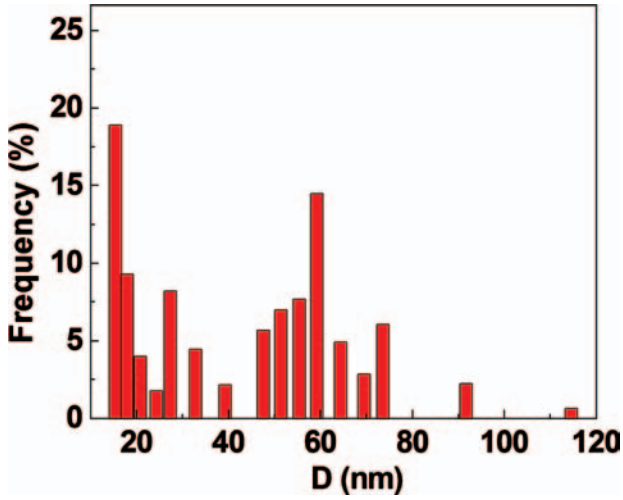

Fig. 1. Size distribution for vanadium oxide nanoparticles.

crystal planes of tetragonal V_2O_5, according to the JCPDS datafile.[15] Figure 3 shows the X-ray diffractogram of the nanoparticles deposited on a Si(111) wafer. This diffractogram agrees with the electron diffraction results. The diffraction peaks are associated to several of the tetragonal V_2O_5 interplanar distances.[15] The linewidth at half maximum leads to an estimate of the typical crystallite size using the Scherrer formula.[16] We find two different linewidths: 23 nm for well formed crystallites and 3 nm for small and disordered ones.

Figure 4 shows the XPS spectrum of the overlapping V_{2p} and O_{1s} binding energy region of the vanadium oxide particles measured on a naturally oxidized silicon substrate. Two partially resolved O_{1s} peaks are seen. One corresponds to vanadium and the other to silicon oxide. We use the O_{1s} peak at 533 eV of silicon oxide[17] for binding energy reference. Surnev et al.[18] conclude that the difference in binding energies between the O_{1s} and $V_{2p3/2}$ level determine the oxidation state of vanadium oxides. This indicates the V^{+5} oxidation state for the nanoparticles, which corresponds to V_2O_5.

Figure 5 shows the UV-Vis spectrum of the vanadium oxide nanoparticle suspension. The light absorption starts in the blue region, giving the suspension the characteristic yellow color. Using the fitting technique described by Escobar-Alarcón et al.,[19] we find an energy gap of 2.2 eV, as shown in the inset nof Figure 5. This gap is associated to V_2O_5.[20]

2.2. Nanoparticle Interaction with Cysteine

Figure 6 shows the nanoparticle size distribution after addition of 1 mg cysteine to the 2 ml suspension. Two distributions around 40 and 130 nm are found, indicating a moderate coalescence of the particles. The pH value of this mixture was measured at 4.5.

Figure 7 shows three UV-Vis spectra in comparison. Spectrum A refers to the vanadium oxide nanoparticle

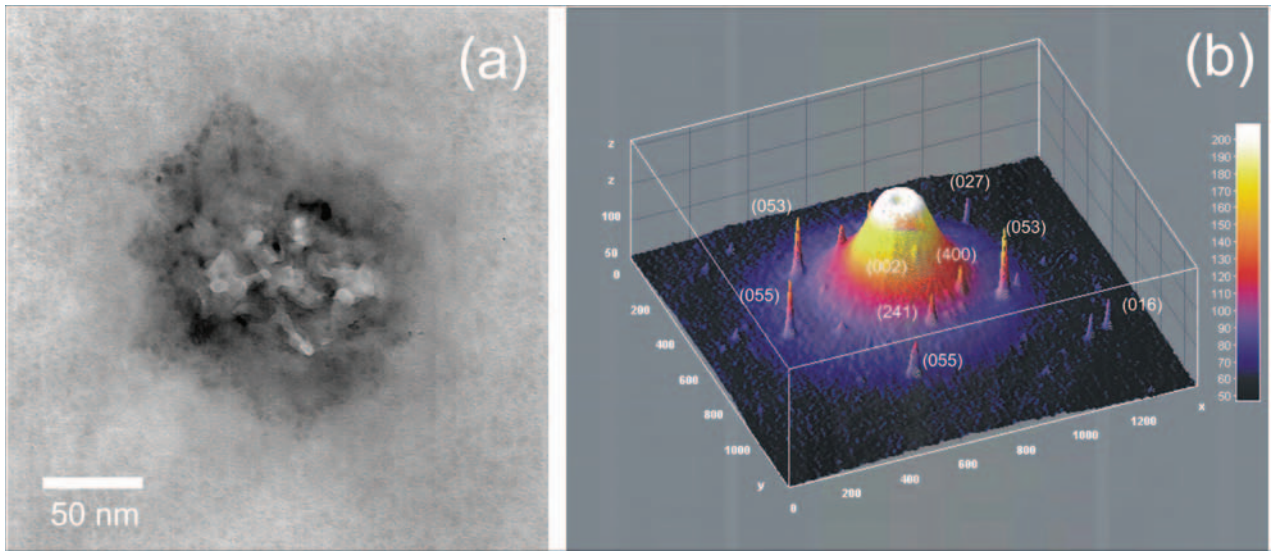

Fig. 2. (a) TEM image of a vanadium oxide nanoparticle obtained by laser ablation in water. (b) 3D view of the electron diffraction pattern of the nanoparticle shown on the left.

suspension, spectrum B to the nanoparticle plus cysteine (0.25 mg/ml) suspension and spectrum C to water dissolved cysteine (5 mg/ml).

Pure cysteine starts to absorb light only in the far UV. The addition of cysteine to the nanoparticle suspension shifts the light absorption from the blue to the UV region (A to B in Fig. 7) and the suspension is visually transparent with a calculated bandgap of 2.87 eV.

In addition to this color shift, a broad absorption band appears at longer wavelengths. We analyzed this part of the spectra in more detail, using several cysteine additions to the vanadium oxide suspension. The plot of the optical absorption at 720 nm versus cysteine concentration is shown in Figure 8. We see a rapid linear increase of the optical absorption at low cysteine concentrations.

At higher cysteine concentrations, typically above 400 μM, the optical absorption has a behavior shown in Figure 9 where two so called isosbestic points are found at 390 and 607 nm.

The investigation of the reaction mechanism between vanadium oxide nanoparticles and cysteine is difficult, since it has to be done in suspension. Additionally, after several hours, especially under illumination, the transparent suspension returns to yellowish. Extra cysteine addition again turns the suspension transparent. Thus, at least

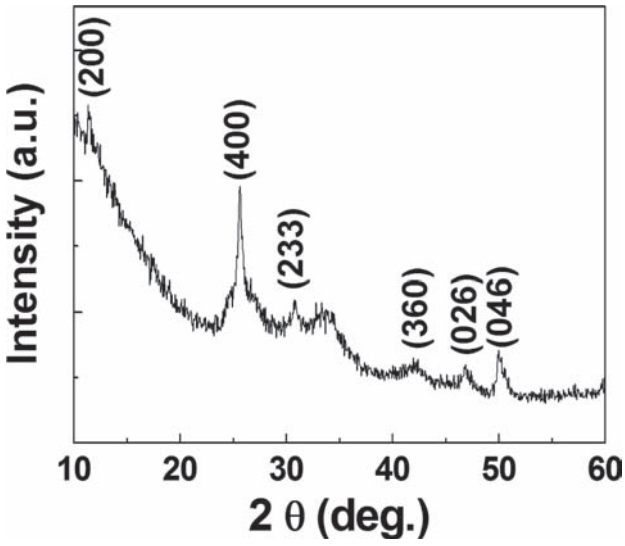

Fig. 3. X-ray diffractogram of vanadium oxide nanoparticles on a Si(111) wafer.

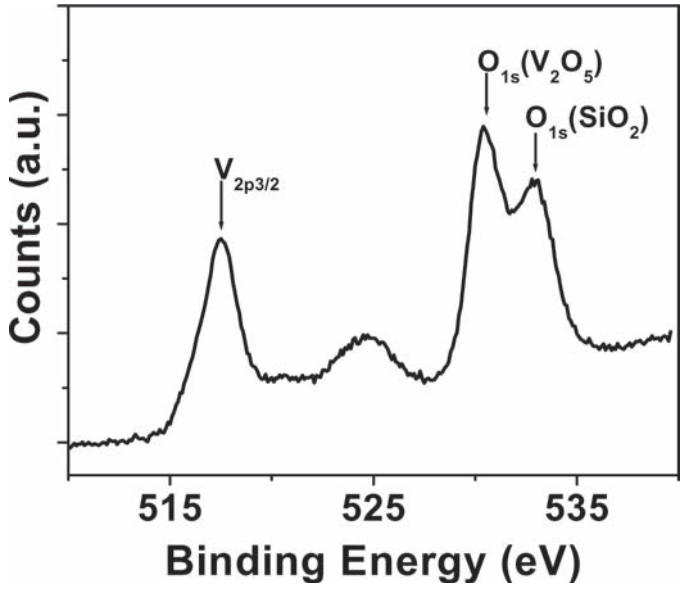

Fig. 4. XPS spectrum of the $V_{2p}O_{1s}$ binding energy region of the vanadium oxide nanoparticles supported on naturally oxidized silicon.

RESEARCH ARTICLE

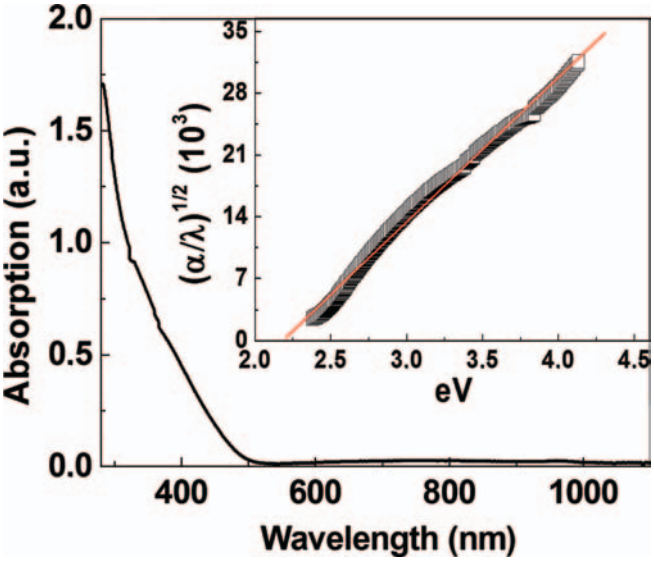

Fig. 5. UV-Vis spectrum of the vanadium oxide nanoparticle suspension. The inset shows the fitting[19] used for bandgap determination.

for the vanadium oxide nanoparticles, the reaction with cysteine seems reversible. Therefore the following XPS findings have to be looked at with care, since they were obtained in a dry state.

The XPS spectrum of pure cysteine (not shown) agreed very well with published results.[21] Figure 10(A) shows a comparison of the N_{1s} binding energy region of pure cysteine (lower) and vanadium oxide reacted cysteine (upper). A clear double peak of the N_{1s} line indicates that the nitrogen atoms are strongly affected by the interaction of the vanadium oxide with cysteine. Figure 10(B) shows a comparison of the S_{2p} binding energy region for pure (lower) cysteine and the reacted (upper) product, showing that the sulphydril sidechain is also affected by the nanoparticle-cysteine interaction. This agrees with findings on metal

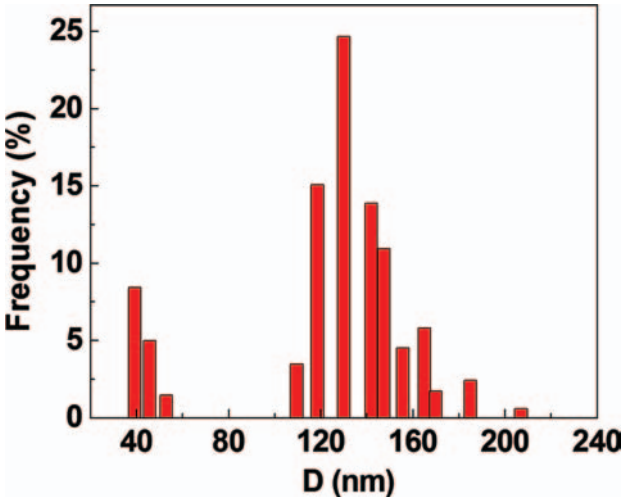

Fig. 6. Size distribution for vanadium oxide nanoparticles interacting with cysteine.

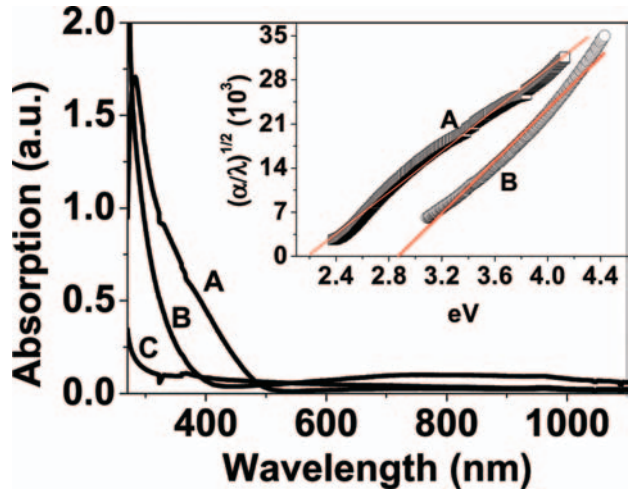

Fig. 7. UV-Vis spectra of: (A) nanoparticle suspension (B) nanoparticle plus cysteine suspension and (C) cysteine. The inset shows the two fittings[19] for bandgap determination.

and other oxide surfaces.[13] The small signal at 168 eV in the upper curve is due to a Si substrate surface plasmon and has no significance in this discussion.

3. DISCUSSION AND CONCLUSIONS

The production of nanoparticles with the LASiS technique, starting with a vanadium target under water, led to tetragonally crystallized V_2O_5 nanoparticles, with sizes distributed around 10 and 60 nm. These could be characterized by DLS,TEM, XRD, XPS and UV-Vis.

The addition of cysteine to the V_2O_5 nanoparticle suspension lead to a color change from yellow to transparent, with a shifting bandgap from 2.2 to 2.87 eV of. Assuming

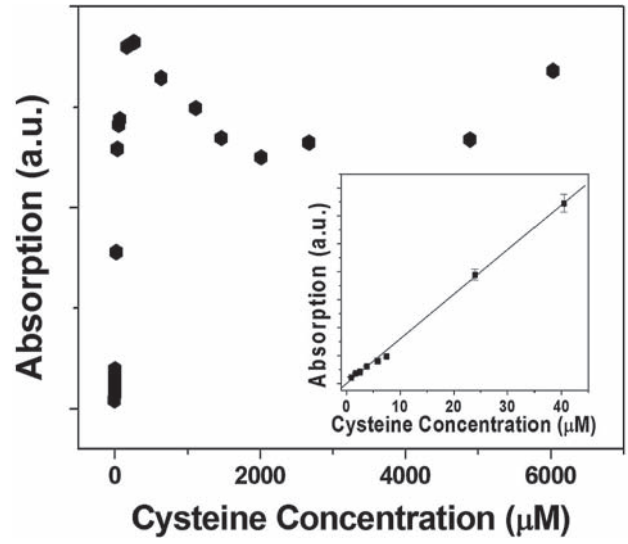

Fig. 8. Optical absorption at the 720 nm wavelength versus cysteine concentration. The inset shows the linear relationship of the absorption versus cysteine concentration at very low concentrations.

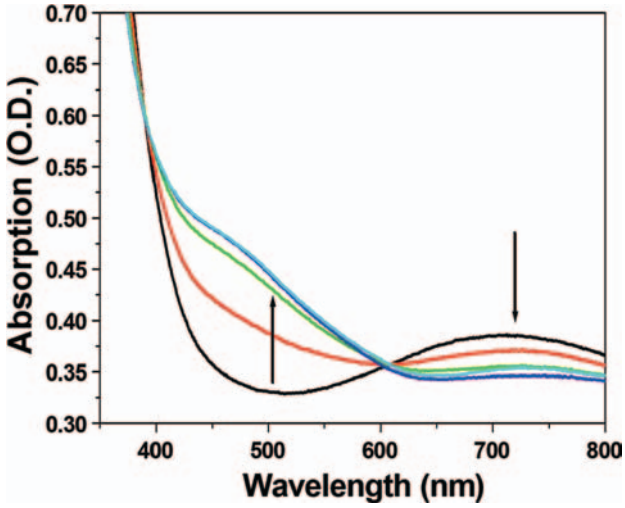

Fig. 9. Light absorption of the vanadium oxide suspension with higher cysteine concentrations. The arrows indicate increasing cysteine concentration.

that V_2O_5, is reduced in this process, this could lead to VO or V_6O_{13} oxides, which have a bandgap, respectively, of 2.8 and 2.7 eV;[22] therefore, cysteine is oxidized.

The large absorption band in the low energy region in the UV-Vis spectra is a signature of ionic systems in two different oxidation states, called the intervalence band. The basic theoretical understanding of this large absorption band phenomenon was done by Hush[23] and later modeled by Piepho, Krausz and Schatz in the so called PKS model, which uses vibronic coupling of mixed valence states.[24, 25] The large optical absorption band thus indicates that V_2O_5 is reduced, probably to two oxides, with vanadium in two valence states. For cysteine concentrations above 400 μM, we find two isosbestic points in the UV-Vis spectra (see Fig. 10) at 390 and 607 nm. These fixed points indicate that two competing absorbing species, probably two oxides, are present in the nanoparticle-cysteine suspension once sufficient cysteine has been added.

Our XPS measurements show that the oxidation of cysteine by the vanadium oxide nanoparticles affects the sulphydril radical and the NH_3 sidechain, since changes in the sulphur and the nitrogen environments of cysteine are seen. In our XPS measurements we have no direct access to the oxi-reduction process, but only to the final dehydrated state.

Pecci et al.[26] describe a copper catalyzed cysteine oxidation with several similar characteristics to our findings. In their case the color change shifts to red. They report a return to the original cuprous complex after complete cysteine consumption. This reversibility is enhanced by oxygen in the suspension. The metal stays in its reduced form during the catalytic process. The thiol sidechain is the reaction site for cysteine oxidation on copper.

Shang et al.[27] report on cysteine detection using fluorescent conjugated polymer stabilized gold nanoparticles.

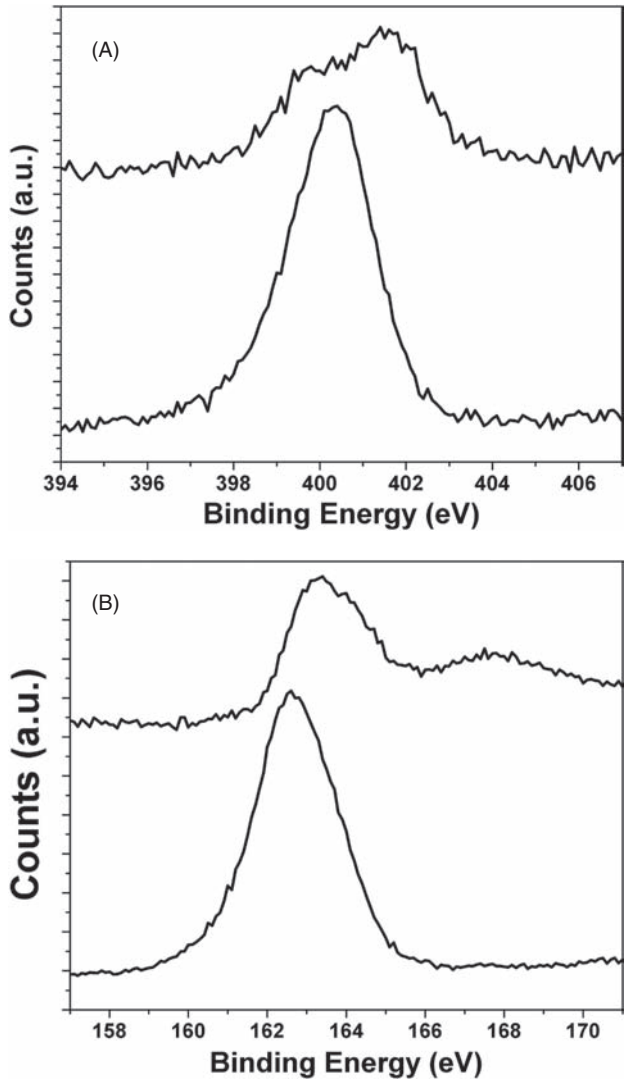

Fig. 10. XPS spectra for the (A) N_{1s} and (B) S_{2p} binding energy region of: pure cysteine (lower) and cysteine reacted with V_2O_5 (upper).

There is a high sensitivity to their method, yet apparently it seems less practical, for the functionalization and stabilization of the gold nanoparticles requires several intermediate steps, whereas our vanadium oxide nanoparticles are produced in one single run.

Nanoparticle size is essential for the color change of V_2O_5 to take place upon addition of cysteine. We tried to reproduce this effect using commercial yellow V_2O_5 powder in water, to no avail.

Additionally, we experimented with all 20 aminoacids, and none, including sulphur containing methionine, showed the color change effect.

This cysteine selectivity is very attractive and, despite the lack of a full comprehension of the oxi-reduction process which occurs, V_2O_5 nanoparticles could be used as simple and effective cysteine sensors. The analysis of the absorption intensity of the intervalence band (see Fig. 9)

indicates that V_2O_5 nanoparticles in suspension can be used to detect cysteine quantities in the μM range.

Acknowledgments: We acknowledge the support of CPqD - Centro de Pesquisa e Desenvolvimento em Telecomunicações and CNPq - Conselho de Desenvolvimento Científico e Tecnológico, Brazilian agencies. Thanks are due to to Laboratório de Polisacarídeos e Carboidratos Vegetais-UFPR for the use of the DLS equipment. of the DLS equipment. Additional acknowledgement is due to our referee, unknown to us, who pointed out the intervalence band absorption in the UV-Vis spectra.

References and Notes

1. H. A. Wriedt, *Journal of Phase Equilibria* 10 **(1989)**.
2. T. Christmann, B. Felde, W. Niesser, D. Schalch, and A. Scharmann, *Thin Sol. Films* 287, 134 **(1996)**.
3. C. G. Granqvist, *Sol. Energy Mater. Solar Cells* 91, 1529 **(2007)**.
4. Y.-S. Lin and C.-W. Tsai, *Surf. Coat. Technol.* 202, 5641 **(2008)**.
5. N. Kambe, S. Kumar, J. T. Gardner, and X. Bi, *USPTO* 6106798, **(2000)**.
6. J. Y. Suh, R. Lopez, L. C. Feldman, and R. F. Haglund, Jr., *J. Appl. Phys.* 96, 1209 **(2004)**
7. F. Krumeich, H.-J. Muhr, M. Niederberger, F. Bieri, B. Schnyder, and R. Nesper, *J. Am. Chem. Soc.* 121, 8324 **(1999)**.
8. M. Niederberger, *Acc. Chem. Res.* 40, 793 **(2007)**.
9. J. Nag and R. F. Haglund, Jr., *J. Phys: Condens. Matter.* 20, 1 **(2008)**.
10. R. Lopez, L. A. Boatner, T. E. Haynes, L. C. Feldman, and R. F. Haglund, Jr., *J. Appl. Phys.* 92, 4031 **(2002)**.
11. J. H. Kim, Y. C. Hong, and H. S. Uhm, *Surf. Coat. Technol.* 201, 5114 **(2007)**.
12. V. Amendola and M. Meneghetti, *Phys. Chem. Chem. Phys.* 11, 3805 **(2009)**.
13. A. Kühnle, T. R. Linderoth, M. Schunack, and F. Besenbacher, *Langmuir* 22, 2156 **(2006)**.
14. XPS International SDP3.2 754 Leona Lane Mountain View California, 94040, USA.
15. JCPDS File-45-1074.
16. B. D. Cullity and R. S. Stock, Elements of X-Ray Diffraction, 3rd edn., Prentice-Hall Inc. **(2001)**, pp. 167–171.
17. J. F. Moulder, W. F. Stickle, P. E. Sobol, and K. D. Bomben, Handbook of X-Ray Photoelectron Spectroscopy, Physical Electronics, Minnesota, USA **(1995)**.
18. S. Surnev, M. G. Ramsey, and F. P. Netze, *Progr. Surf. Sci.* 73, 117 **(2003)**
19. L. Escobar-Alarcón, A. Arrieta, E. Camps, S. Muhl, S. Rodil, and E. Vigueras-Santiago, *Appl. Surf. Science* 254, 412 **(2007)**.
20. L.-J. Meng R. A. Silva, H.-N. Cui, V. Teixeira, M. P. dos Santos, and Z. Zheng Xu, *Thin Sol. Films* 515, 195 **(2006)**.
21. R. A. Brizzolara, *Surf. Sci. Spectra* 4, 107.
22. C. A. P. Andrade, Crecimiento y caracterización de películas delgadas de VO, V_6O_{13}y VO_2 por sputtering magnetron DC. Master's Thesis, Universidad de Puerto Rico, Mayaguëz **(2006)**.
23. (a) N. S. Hush, *Prog. Inorg. Chem.* 8, 391 **(1967)**; (b) *Electrochim. Acta* 13, 1005 **(1968)**.
24. S. B. Piepho, E. R. Krausz, and P. N. Schatz, *J. Am. Chem. Soc.* 100, 2996 **(1978)**.
25. K. Y. Wong, P. N. Schatz, and S. B. Piepho, *J. Am. Chem. Soc.* 101, 2793 **(1979)**.
26. L. Pecci, G. Montefoschi, G. Musci, and D. Cavallini, *Amino Acids* 13, 355 **(1997)**.
27. L. Shang, C. Qin, T. Wang, M. Wang, L. Wang, and S. Dong, *J. Phys. Chem.* 111, 13414 **(2007)**.

Received: 21 March 2010. Accepted: 25 November 2010.

RESEARCH ARTICLE